The Journal of Chemical Physics

RESEARCH ARTICLE | NOVEMBER 06 2023

Hydrogen-mediated polarity compensation on the (110) surface terminations of ABO_3 perovskites

Victor Fung ; Guoxiang Hu ; Zili Wu ; De-en Jiang

J. Chem. Phys. 159, 174706 (2023)
https://doi.org/10.1063/5.0161435

The Journal of Chemical Physics ARTICLE pubs.aip.org/aip/jcp

Hydrogen-mediated polarity compensation on the (110) surface terminations of ABO_3 perovskites

Cite as: J. Chem. Phys. 159, 174706 (2023); doi: 10.1063/5.0161435
Submitted: 10 June 2023 • Accepted: 17 October 2023 •
Published Online: 6 November 2023

Victor Fung,[1,a] Guoxiang Hu,[1,b] Zili Wu,[1,2] and De-en Jiang[3,4,c]

AFFILIATIONS

[1] Center for Nanophase Materials Sciences, Oak Ridge National Laboratory, Oak Ridge, Tennessee 37831, USA
[2] Chemical Sciences Division, Oak Ridge National Laboratory, Oak Ridge, Tennessee 37831, USA
[3] Department of Chemistry, University of California, Riverside, California 92521, USA
[4] Department of Chemical and Biomolecular Engineering, Vanderbilt University, Nashville, Tennessee 37235, USA

[a] **Present address:** School of Computational Science and Engineering, Georgia Institute of Technology, Atlanta, Georgia 30332, USA.
[b] **Present address:** School of Materials Science and Engineering, Georgia Institute of Technology, Atlanta, Georgia 30332, USA
[c] **Author to whom correspondence should be addressed:** de-en.jiang@vanderbilt.edu

ABSTRACT

Polar surfaces undergo polarity compensation, which can lead to significantly different surface chemistry from their nonpolar counterparts. This process in turn can substantially alter the binding of adsorbates on the surface. Here, we find that hydrogen binds much more strongly to the polar (110) surface than the nonpolar (100) surface for a wide range of ABO_3 perovskites, forming a hydroxyl layer on the O_2^{4-} termination and a hydride layer on the ABO^{4+} termination of the (110) surface. The stronger adsorption on the polar surfaces can be explained by polarity compensation: hydrogen atoms can act as electron donors or acceptors to compensate for the polarity of perovskite surfaces. The relative stability of the surface terminations is further compared under different gas environments and several perovskites have been found to form stable surface hydride layers under oxygen-poor conditions. These results demonstrate the feasibility of creating stable surface hydrides on perovskites by polarity compensation which might lead to new hydrogenation catalysts based on ABO_3 perovskites.

I. INTRODUCTION

Polar surfaces arise when crystals are cleaved to form layers with a non-zero dipole moment. These layers experience a diverging electrostatic potential leading to an infinitely high surface energy with layer thickness, also known as "polar catastrophe."[1,2] To counteract this effect, surfaces undergo polarity compensation to cancel the polarity, which can take the form of geometric reconstruction of surface atoms, electronic/charge redistribution, and the adsorption of foreign atoms or molecules.[3–10] Consequently, the surface chemistry of polar surfaces may differ significantly from nonpolar ones, presenting an opportunity to design surfaces which are stabilized by the need for polarity compensation.

Complex oxides such as ABO_3 perovskites are technologically important and frequently have polar surfaces. For example, $SrTiO_3$ (STO), one of the most studied ABO_3 perovskites, has a slightly polar (100) surface and polar (110) and (111) surfaces. By modifying the synthesis conditions, one can prepare STO nanoparticles with predominantly (100) or (110) surfaces which show significantly varying catalytic properties.[11–14] The polar STO(110) surface is prone to geometric reconstructions, as revealed from experimental and theoretical studies.[15–17] Alternatively, surface adsorbates such as H_2O have been well-demonstrated to achieve polarity compensation *in lieu* of geometric reconstruction in oxides such as MgO[18] and more specifically for perovskites such as $KTaO_3$.[19] But it is unclear if other adsorbates could also accomplish the same effect in

adsorbate-mediated polarity compensation on the perovskite (110) surface.

Hydrogen is a ubiquitous adsorbate in catalysis.[20–27] On metal oxides, hydrogen can be found bound to oxygen as hydroxyl groups but can also be found to adsorb on metal sites as hydrides.[28] Hydrides can also replace lattice oxygen in perovskites to form perovskite oxyhydrides.[29–31] The unique flexibility in the charge state of the hydrogen allows it to be responsible for both electron donation and withdrawal, which is accompanied by significant differences in their chemistry. For example, hydrides are hypothesized to play a crucial role in the exceptional catalytic activity present in electrides and oxyhydrides for ammonia synthesis and selective hydrogenation.[32–38] Therefore, we are motivated to understand the formation and stability of hydrides on the surfaces of ABO_3 perovskites from the perspective of polarity compensation. We focus on STO (110) and then extend to other perovskite (110) surfaces. We show indeed that polarity compensation can be used to control the charge state of the hydrogen, leading to stable surface hydrides which could be potentially used for hydrogenation catalysis. Below we first explain the computational method and the surface models.

II. METHODS

Density functional theory (DFT) calculations were carried out using the Vienna *ab initio* Simulation Package (VASP).[39,40] The Perdew–Burke–Ernzerhof (PBE)[41] functional form of generalized-gradient approximation (GGA) for electron exchange and correlation energies were used with the D3 van der Waals correction included.[42] All calculations were performed with spin polarization. The projector-augmented wave method was used to describe the electron-core interaction[39,43] with a kinetic energy cutoff of 450 eV for the surface calculations. A 6 × 6 × 1 sampling of Brillouin zone using a Monkhorst–Pack scheme was used for the k-points.[44] A convergence criterion of 10^{-4} eV was used for electronic self-consistency of the total energy, and 10^{-3} eV/Å was used for ionic relaxation. A vacuum layer of 20 Å was created for the surface slabs; the slab contains a total of nine layers, with the middle layer of the surface slab fixed in the calculations. The remaining atoms in the slab were relaxed during geometry optimization. Charge densities and isosurfaces were visualized using VESTA.[45]

The hydrogen absorption energy (E_H) is calculated from the equation $E_H = E_{surface+H} - (E_{pristine\text{-}surface} + \frac{1}{2} E_{H2})$. The energy of E_{H2} was computed by placing the H_2 adsorbate in a cubic cell with a 15 Å wide vacuum in each direction. The symmetric (110) slabs used in this work are stochiometric with respect to the A and B atoms, differing only by the O count, which allows for the surface energy to be obtained as a function of μ_O and μ_H. For the (100) slab, a non-symmetric stab with both TiO_2 and SrO terminations is used, which yields an average surface energy for the two terminations. We investigated the impact of strong electron localization on transition metals via DFT+U calculations (using a U value of 4.45 obtained from a previous study[46]) and found that the impact of U on E_H is relatively minor (within 0.1 eV between GGA+U and GGA).

III. RESULTS AND DISCUSSION

We first examine in detail H adsorption on STO (100) and (110) surfaces. From the adsorption energetics, geometry, and electronic structure, we reveal the chemical nature of the interaction of H with different surfaces that we then extend to other ABO_3 perovskites.

A. H adsorption on STO (100) and (110)

The bulk STO has a cubic structure [Fig. 1(a)] and is a semiconductor [Fig. 1(b)]. The (100) and (110) surfaces are two common low-index terminations which can be cleaved from the bulk ABO_3 perovskite [Fig. 1(a)]. (100) and (110) surfaces of cubic STO both have two distinct terminations. For (100) the terminations contain either an SrO layer or a TiO_2 layer on the surface, whereas for (110) the terminations contain an $SrTiO^{4+}$ layer or an O_2^{4-} layer [Figs. 1(c) and 1(d)]. Based on formal charges, SrO and TiO_2 are neutral (with the cations in the oxidation states Sr^{2+} and Ti^{4+}), so the (100) surface is considered a formally nonpolar surface. Meanwhile, STO(110) $SrTiO^{4+}$ and O_2^{4-} terminations are formally polar surfaces. We note that the actual partial charges (obtained from a particular charge partition scheme such as Bader charges) of the SrO and TiO_2 layers are not zero and (100) terminations are in reality slightly polar surfaces.[1,47] Nonetheless the (100) and (110) surfaces are sufficiently different in electronic structure and chemistry such that a broad distinction in terms of their polarity can still be made, as we will illustrate below.

We start by comparing hydrogen adsorption energies between the (100) and (110) surfaces at 100% coverage of surface sites in Fig. 2. On the (100) SrO termination, hydrogen has only one adsorption site available at the lattice oxygen site, with a binding energy of −0.15 eV relative to $\frac{1}{2}$ H_2 [Fig. 2(b)]. The (110) O_2^{4-} termination is also characterized by having the lattice oxygen as the only adsorption site, but with an unusually high binding energy of −2.56 eV [Fig. 2(d)]. On the (100) TiO_2 termination, hydrogen can adsorb on the O or Ti site with a strong preference to O. On the (110) $SrTiO^{4+}$ termination, the trend is reversed: hydrogen strongly prefers the Ti site instead of the O site with a favorable energy of −0.46 eV [Fig. 2(c)]. To compare the Ti–H binding between (100) and (110), we also computed the H adsorption energy on the Ti site of the (100) TiO_2 termination which was found to be highly unfavorable [+2.10 eV, Fig. 2(a)] than on the O site of the (100) TiO_2 (0.65 eV). In addition, we evaluated dipole correction on the STO(100) surface to account for the slightly polar nature of the surface and found that its impact on H adsorption energy is minimal (within 0.01 eV). We see quite clearly that on the (110) terminations, Ti–H and O–H bindings are stronger than their (100) counterparts to an unusually high degree, both by roughly 2.5 eV: −0.46 eV vs +2.10 eV for H–Ti; −2.56 eV vs −0.15 eV for H–O.

To understand the energetic difference between STO (100) and (110) toward H adsorption, we next examine the density of states (DOS) of each termination before and after H adsorption. On the STO(100) TiO_2 termination, Ti–H bonding is characterized by a negligible degree of charge transfer from the H to Ti. As a result, the DOS is largely unchanged before and after adsorption [Fig. 2(a)], with the surface maintaining its electronic band gap similar to that of the bulk [Fig. 1(b)]. On the STO(100) SrO termination, the O–H bonding is characterized by an unfavorable reduction of the STO;

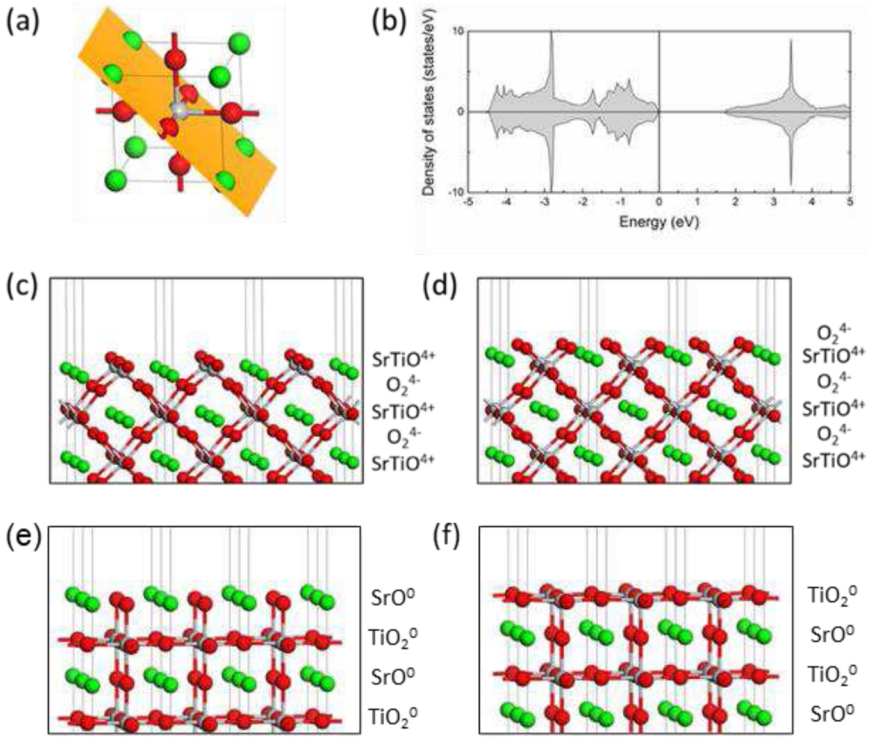

FIG. 1. (a) Atomistic model of the model perovskite $SrTiO_3$ and the (110) cleavage plane on the $SrTiO^{4+}$ termination. (b) Density of states of bulk $SrTiO_3$. (c) Side-view of the (110) $SrTiO^{4+}$-terminated surface. (d) Side-view of the (110) $O_2{}^{4-}$-terminated surface. (e) Side-view of the (100) SrO-terminated surface. (f) Side-view of the (100) TiO_2-terminated surface. Ti, gray; O, red; Sr, green.

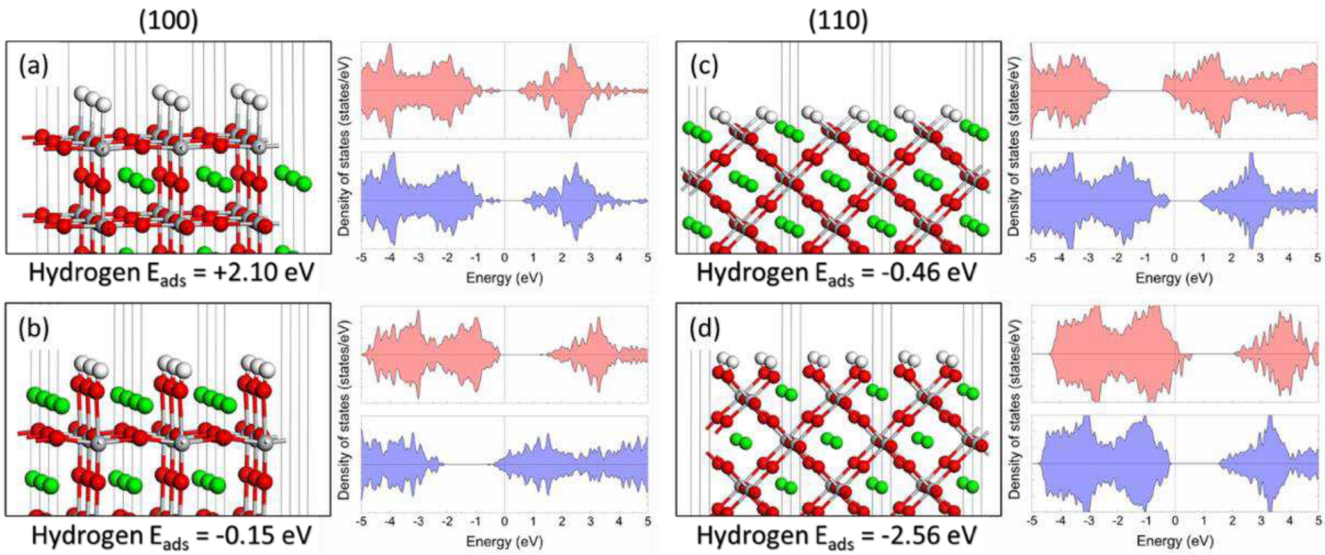

FIG. 2. Atomistic models and density of states before (red) and after (blue) hydrogen adsorption: (a) on Ti of the (100) TiO_2 termination; (b) on O of the (100) SrO termination; (c) on Ti of the (110) $SrTiO^{4+}$ termination; (d) on O of the (110) $O_2{}^{4-}$ termination. Ti, gray; O, red; Sr, green; H, white.

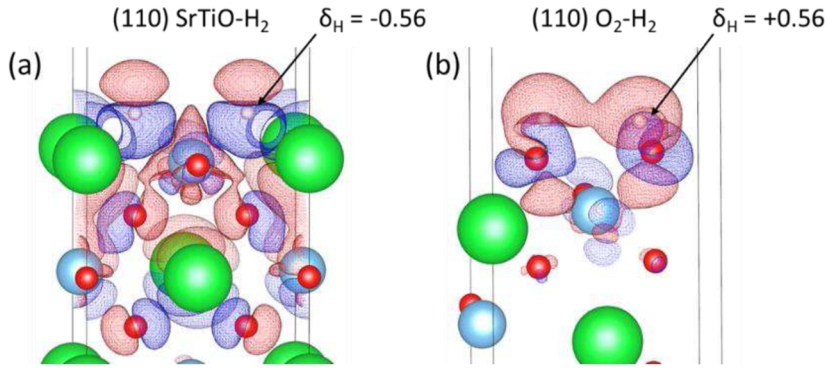

FIG. 3. Charge density difference between hydrogen adsorption on the surface and isolated H and the clean surface: (a) on (110) $SrTiO^{4+}$ termination; (b) on (110) O_2^{4-} termination. Blue, electron accumulation; red, electron depletion.

here the electrons are transferred from the hydrogen to the antibonding states of the surface which can be observed by an upshift of the Fermi level to the conduction band [Fig. 2(b)].[24] In contrast, the situation is markedly different for STO(110): H on the O_2^{4-} termination (via formation of H–O bond) donates its electron to fill the valence band [Fig. 2(d)]; H on the (110) $SrTiO^{4+}$ termination (via the H–Ti bonding) accepts or depletes the electron from the conduction band by the transfer and localization of excess charge onto the hydrogen to form hydrides [Fig. 2(c)]. Both charge transfer processes for O–H and Ti–H bonding on STO (110) are favorable and return the surface to a semiconducting bulk-like state, which explains the much stronger binding energy of hydrogen on these surfaces. Bader charges and the charge density difference plot (Fig. 3) agree with this observation: H atoms are negatively charged at −0.56 e on the (110) $SrTiO^{4+}$ termination [Fig. 3(a)] and positively charged at 0.56 e on the (110) O_2^{4-} termination [Fig. 3(b)].

B. Effect of gas environment on the surface stability

The results above have focused on a full coverage of H on the surfaces and the corresponding H adsorption energies. It is more informative to compare their stability by using first principles thermodynamics to evaluate the surface energy with varying gas environments. The surface energy of the ABO_3 perovskite (γ defined in this work is calculated from the equation:

$$\gamma(T,p) = \frac{1}{2S_A}\Big[E_{slab} - N_A E_{bulk} + (3N_A - N_O)\frac{1}{2}E_{O_2} - N_H\frac{1}{2}E_{H_2} + (3N_A - N_O)\mu_O - N_H\mu_H\Big],$$

where S_A is the surface area of the slab, E_{slab} the energy of the slab; N_A, N_H, N_O the numbers of A, H, and O atoms in the slab; E_{bulk} the energy of bulk ABO_3; E_{O_2} the energy of an O_2 molecule; μ_O, μ_H the chemical potentials of O, H atoms, respectively. Figure 4 shows the surface energies of the pristine and H-covered (100) and (110) surfaces at various μ_O and a fixed μ_H corresponding to ~1 atm H_2 partial pressure at 400 K. One can see that the H-covered (110) O_2^{4-} terminated surface has the lowest surface energy; in other words, polarity compensation by H adsorption greatly stabilizes the STO(110) O_2^{4-} termination than the other (110) and (100) terminations.

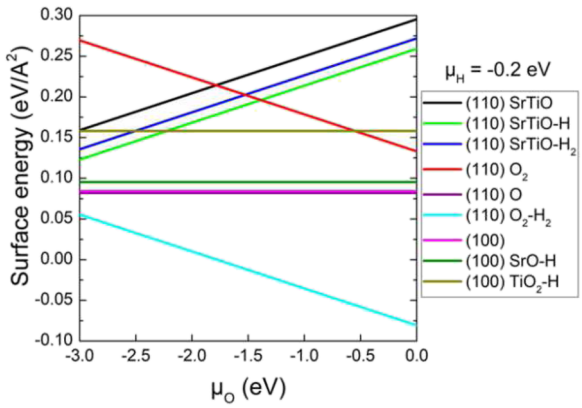

FIG. 4. Surface energy as a function of oxygen chemical potential (where $\mu_O = -0.3$ eV corresponds to ~1 atm O_2 partial pressure at 300 K) at constant temperature and hydrogen chemical potential ($\mu_H = -0.2$ eV, corresponding to ~1 atm H_2 partial pressure at 300 K) for different terminations of pristine and adsorbed STO (100) and (110) surfaces. The (110) O surface refers to a termination with half the oxygen sites being vacant.

C. Generalization to (110) surfaces of other perovskites

Hydrogen-adsorption-induced polarity compensation on a polar surface is a novel finding from the present work. To see how general this finding is, we have examined H adsorption on the (110) surface of a diverse set of 26 other stable ABO_3 perovskites, including cubic and orthorhombic structures, different oxidation states, and varying electronic structure from insulating to metallic. While these perovskites are just a subset of possible stable perovskites, it amply represents a broad sampling of different possible chemical compositions and properties. Figure 5(a) compares the pristine ABO and O_2 terminations of the ABO_3 (110)

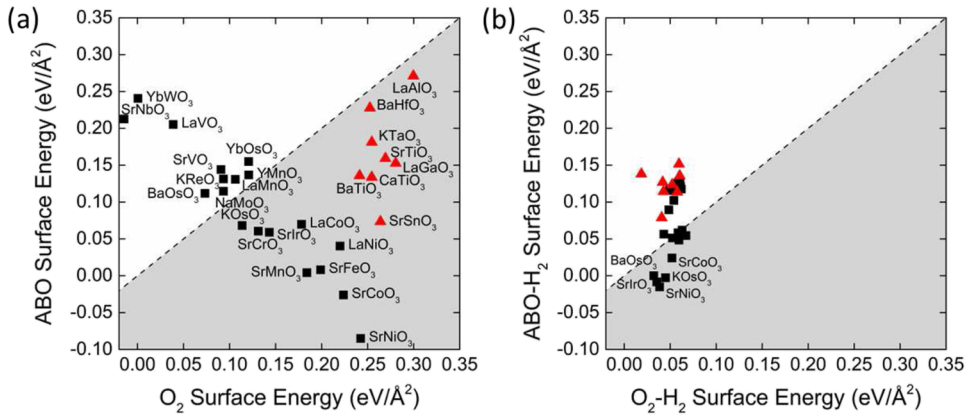

FIG. 5. Surface energies of ABO_3 perovskite (110) ABO^{4+} termination vs O_2^{4-} termination: (a) pristine terminations ($\mu_O = -3$ eV, $\mu_H = -0.2$ eV); (b) H-adsorbed terminations ($\mu_O = -3$ eV, $\mu_H = -0.2$ eV). Gray region: ABO^{4+} termination more stable; white region: O_2^{4-} termination more stable. Black squares: perovskites which are conductive; red triangles, perovskites which have a band gap. See Table S1 for the values in (a) and Fig. S1(a) for the full labels in (b) in the supplementary material.

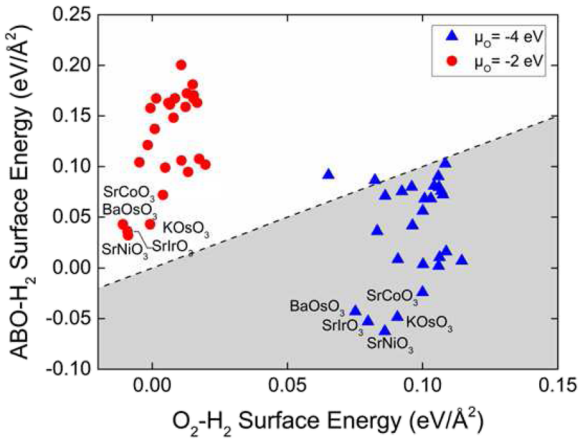

FIG. 6. Surface energies of H-adsorbed ABO_3(110) ABO^{4+} termination vs O_2^{4-} termination at various O chemical potentials and fixed $\mu_H = -0.2$ eV. Gray region: ABO^{4+} termination more stable; white region: O_2^{4-} termination more stable. See Fig. S1(b) and Table S2 in the supplementary material for the full labels and values.

surfaces by plotting their surface energies. For perovskites which are conductive [that is, having a non-zero electronic density of states at the Fermi level; black squares in Fig. 5(a)], there is an apparent inverse correlation between the surface energies of ABO^{4+} and O_2^{4-} terminations: surfaces with the most stable ABO^{4+} termination tend to have the least stable O_2^{4-} termination, and vice versa. The perovskites which have a band gap [red triangles in Fig. 5(a)], however, follow a different trend: their ABO^{4+} terminations vary greatly in surface energy, but their O_2^{4-} terminations all have a similar, high surface energy. Figure 5(b) shows the relative stability of the ABO^{4+} vs O_2^{4-} termination after H adsorption. Moving to the hydrogen-covered (110) surfaces reveals an overall reduction in surface energies compared to the pristine (110) surface, demonstrating the general effect of hydrogen-mediated polarity compensation across the perovskites. In most cases, the reduction in surface energy from hydrogen adsorption is greatest on surfaces which have the highest surface energy in the pristine form, with the insulating perovskites in particular exhibiting this phenomenon ($LaAlO_3$, $BaHfO_3$, $KTaO_3$, $SrTiO_3$, $LaGaO_3$, $CaTiO_3$, $BaTiO_3$, and $SrSnO_3$).

D. Hydride-forming ABO_3(110) surfaces

Figure 5 above demonstrated polarity compensation from H adsorption in stabilizing especially the O_2^{4-} termination via forming the OH groups on the ABO_3(110) surfaces at the conditions of $\mu_O = -3$ eV and $\mu_H = -0.2$ eV. We have further examined the effect of varying O chemical potentials on the relative stability of H-adsorbed ABO_3(110) terminations, to search for stable surface hydride-forming perovskites. As shown in Fig. 6, the hydrogen-covered O_2^{4-} termination is most stable under oxygen-rich conditions where $\mu_O = -2$ eV (red circles), and the hydride-covered ABO^{4+} termination is most stable under oxygen-poor conditions where $\mu_O = -4$ eV (blue triangles). This switch in surface termination preference is particularly relevant for catalysis which span a wide range of μ_O depending on the reaction conditions. Our search across the perovskites also reveals a number of candidates ($BaOsO_3$, $SrIrO_3$, $SrNiO_3$, $KOsO_3$, $SrCoO_3$) which exhibit more stable hydride-forming ABO^{4+} terminations than the hydroxyl-covered O_2^{4-} terminations under reducing conditions at 300 K where $\mu_O < -3$ eV for their (110) surfaces. Table I shows that H adsorption is indeed very favorable on the ABO^{4+} terminations of the (110) surfaces of those perovskites. In other words, we predict that the perovskites in Table I will have more stable H-covered ABO^{4+} terminations (via surface hydride or H–Ti bond formation) than the H-covered O_2^{4-} terminations for the (110) surfaces under oxygen-poor conditions.

We note that the present findings are based on the DFT-PBE results for mainly the (110) surfaces of ABO_3 perovskites. Although we found that the PBE + U method gives the same trends as the corrections to the surface energies and adsorption energies are within

TABLE I. Hydrogen adsorption energies (E_{ads}) on the ABO^{4+} terminations of the (110) surfaces of likely hydride-forming perovskites, based on the criterion that hydride-forming ABO^{4+} terminations are stable than the hydroxyl-covered O_2^{4-} terminations under reducing conditions ($\mu_O < -3$ eV at 300 K).

Perovskite	E_{ads} (eV)
$BaOsO_3$	−0.68
$SrIrO_3$	−1.41
$SrNiO_3$	−2.35
$KOsO_3$	−0.95
$SrCoO_3$	−1.99

0.10 eV, such corrections to account for the strongly localized states and other factors such as spin–orbit coupling might lead to larger energetic variations that could impact the applicability of the present conclusions to more complex oxides and their surface terminations. Further studies are warranted.

IV. SUMMARY AND CONCLUSIONS

We have examined H adsorption on the different terminations of the polar (110) surfaces of ABO_3 perovskites with density functional theory. We found that polarity compensation strongly influences H adsorption, leading to a hydroxyl layer on the O_2^{4-} termination by filling holes in the valence band and a hydride layer on the ABO^{4+} termination by removal of electrons in the conduction band on the ABO^{4+} termination. Under the relatively oxidizing conditions, the H-covered O_2^{4-} termination is more stable, while under more reducing conditions, the ABO^{4+} termination with a surface hydride layer is more stable. Perovskites with the greatest tendency to form surface hydrides on the (110) ABO^{4+} termination have been identified. Our findings reveal the potential of creating stable surface hydrides on ABO_3 perovskites for catalysis.

SUPPLEMENTARY MATERIAL

See the supplementary material for surface energies of clean and hydrogen-covered terminations of various ABO_3(110) surfaces.

ACKNOWLEDGMENTS

This work was sponsored by the U.S. Department of Energy, Office of Science, Office of Basic Energy Sciences, Chemical Sciences, Geosciences, and Biosciences Division, Catalysis Science Program. This research used resources of the National Energy Research Scientific Computing Center, a DOE Office of Science User Facility supported by the Office of Science of the U.S. Department of Energy under Contract No. DE-AC02-05CH11231.

AUTHOR DECLARATIONS

Conflict of Interest

The authors have no conflicts to disclose.

Author Contributions

Victor Fung: Conceptualization (lead); Data curation (lead); Formal analysis (lead); Investigation (lead); Writing – original draft (lead). **Guoxiang Hu**: Investigation (supporting); Writing – review & editing (supporting). **Zili Wu**: Funding acquisition (supporting); Project administration (supporting); Supervision (supporting); Writing – review & editing (supporting). **De-en Jiang**: Funding acquisition (lead); Project administration (lead); Writing – review & editing (lead).

DATA AVAILABILITY

The data that support the findings of this study are available from the corresponding author upon reasonable request.

REFERENCES

[1] C. Noguera, "Polar oxide surfaces," J. Phys.: Condens. Matter **12**, R367–R410 (2000).
[2] J. Goniakowski, F. Finocchi, and C. Noguera, "Polarity of oxide surfaces and nanostructures," Rep. Prog. Phys. **71**, 016501 (2007).
[3] R. Pentcheva and W. E. Pickett, "Avoiding the polarization catastrophe in $LaAlO_3$ overlayers on $SrTiO_3$ through polar distortion," Phys. Rev. Lett. **102**, 107602 (2009).
[4] O. Dulub, U. Diebold, and G. Kresse, "Novel stabilization mechanism on polar surfaces: ZnO(0001)–Zn," Phys. Rev. Lett. **90**, 016102 (2003).
[5] A. F. Santander-Syro, O. Copie, T. Kondo, F. Fortuna, S. Pailhès, R. Weht, X. G. Qiu, F. Bertran, A. Nicolaou, A. Taleb-Ibrahimi, P. Le Fèvre, G. Herranz, M. Bibes, N. Reyren, Y. Apertet, P. Lecoeur, A. Barthélémy, and M. J. Rozenberg, "Two-dimensional electron gas with universal subbands at the surface of $SrTiO_3$," Nature **469**, 189 (2011).
[6] C. F. Chang, Z. Hu, S. Klein, X. H. Liu, R. Sutarto, A. Tanaka, J. C. Cezar, N. B. Brookes, H. J. Lin, H. H. Hsieh, C. T. Chen, A. D. Rata, and L. H. Tjeng, "Dynamic atomic reconstruction: How Fe_3O_4 thin films evade polar catastrophe for epitaxy," Phys. Rev. X **6**, 041011 (2016).
[7] M. Capdevila-Cortada and N. López, "Entropic contributions enhance polarity compensation for CeO_2(100) surfaces," Nat. Mater. **16**, 328 (2016).
[8] J. Goniakowski and C. Noguera, "Microscopic mechanisms of stabilization of polar oxide surfaces: Transition metals on the MgO(111) surface," Phys. Rev. B **66**, 085417 (2002).
[9] R. Wahl, J. V. Lauritsen, F. Besenbacher, and G. Kresse, "Stabilization mechanism for the polar ZnO(0001)–O surface," Phys. Rev. B **87**, 085313 (2013).
[10] Z. Wang, M. Reticcioli, Z. Jakub, I. Sokolović, M. Meier, L. A. Boatner, M. Schmid, G. S. Parkinson, U. Diebold, C. Franchini, and M. Setvin, "Surface chemistry on a polarizable surface: Coupling of CO with $KTaO_3$(001)," Sci. Adv. **8**, eabq1433 (2022).
[11] F. Polo-Garzon, S.-Z. Yang, V. Fung, G. S. Foo, E. E. Bickel, M. F. Chisholm, D.-e. Jiang, and Z. Wu, "Controlling reaction selectivity through the surface termination of perovskite catalysts," Angew. Chem., Int. Ed. **56**, 9820–9824 (2017).
[12] G. S. Foo, Z. D. Hood, and Z. Wu, "Shape effect undermined by surface reconstruction: Ethanol dehydrogenation over shape-controlled $SrTiO_3$ nanocrystals," ACS Catal. **8**, 555–565 (2018).
[13] Z. Bao, V. Fung, F. Polo-Garzon, Z. D. Hood, S. Cao, M. Chi, L. Bai, D.-e. Jiang, and Z. Wu, "The interplay between surface facet and reconstruction on isopropanol conversion over $SrTiO_3$ nanocrystals," J. Catal. **384**, 49–60 (2020).
[14] Q. Jia, C. Wang, J. Liu, X. Cai, L. Zhong, G. Yu, and D. Duan, "Strong synergistic effect of the (110) and (100) facets of the $SrTiO_3$ perovskite micro/nanocrystal: Decreasing the binding energy of exciton and superb photooxidation capability for Co^{2+}," Nanoscale **14**, 12875–12884 (2022).
[15] Z. Wang, A. Loon, A. Subramanian, S. Gerhold, E. McDermott, J. A. Enterkin, M. Hieckel, B. C. Russell, R. J. Green, A. Moewes, J. Guo, P. Blaha, M. R. Castell, U. Diebold, and L. D. Marks, "Transition from reconstruction toward thin film on the (110) surface of strontium titanate," Nano Lett. **16**, 2407–2412 (2016).

[16]M. Riva, M. Kubicek, X. Hao, G. Franceschi, S. Gerhold, M. Schmid, H. Hutter, J. Fleig, C. Franchini, B. Yildiz, and U. Diebold, "Influence of surface atomic structure demonstrated on oxygen incorporation mechanism at a model perovskite oxide," Nat. Commun. **9**, 3710 (2018).
[17]J. A. Enterkin, A. K. Subramanian, B. C. Russell, M. R. Castell, K. R. Poeppelmeier, and L. D. Marks, "A homologous series of structures on the surface of $SrTiO_3$(110)," Nat. Mater. **9**, 245 (2010).
[18]B. E. Gaddy, E. A. Paisley, J.-P. Maria, and D. L. Irving, "Overcoming the polarization catastrophe in the rocksalt oxides MgO and CaO," Phys. Rev. B **90**, 125403 (2014).
[19]M. Setvin, M. Reticcioli, F. Poelzleitner, J. Hulva, M. Schmid, L. A. Boatner, C. Franchini, and U. Diebold, "Polarity compensation mechanisms on the perovskite surface $KTaO_3$(001)," Science **359**, 572–575 (2018).
[20]J. K. Nørskov, J. Rossmeisl, A. Logadottir, L. Lindqvist, J. R. Kitchin, T. Bligaard, and H. Jonsson, "Origin of the overpotential for oxygen reduction at a fuel-cell cathode," J. Phys. Chem. B **108**, 17886–17892 (2004).
[21]J. Greeley, T. F. Jaramillo, J. Bonde, I. Chorkendorff, and J. K. Nørskov, "Computational high-throughput screening of electrocatalytic materials for hydrogen evolution," Nat. Mater. **5**, 909–913 (2006).
[22]A. A. Latimer, A. R. Kulkarni, H. Aljama, J. H. Montoya, J. S. Yoo, C. Tsai, F. Abild-Pedersen, F. Studt, and J. K. Nørskov, "Understanding trends in C–H bond activation in heterogeneous catalysis," Nat. Mater. **16**, 225–229 (2017).
[23]V. Fung, F. F. Tao, and D. E. Jiang, "General structure-reactivity relationship for oxygen on transition-metal oxides," J. Phys. Chem. Lett. **8**, 2206–2211 (2017).
[24]V. Fung, Z. Wu, and D.-e. Jiang, "New bonding model of radical adsorbate on lattice oxygen of perovskites," J. Phys. Chem. Lett. **9**, 6321–6325 (2018).
[25]C. Coperet, "C–H bond activation and organometallic intermediates on isolated metal centers on oxide surfaces," Chem. Rev. **110**, 656–680 (2010).
[26]J. Moon, Y. Cheng, L. L. Daemen, M. Li, F. Polo-Garzon, A. J. Ramirez-Cuesta, and Z. Wu, "Discriminating the role of surface hydride and hydroxyl for acetylene semihydrogenation over ceria through *in situ* neutron and infrared spectroscopy," ACS Catal. **10**, 5278–5287 (2020).
[27]S. K. M. Padavala and K. A. Stoerzinger, "Role of hydride formation in electrocatalysis for sustainable chemical transformations," ACS Catal. **13**, 4544–4551 (2023).
[28]J. Kammert, J. Moon, and Z. Wu, "A review of the interactions between ceria and H_2 and the applications to selective hydrogenation of alkynes," Chin. J. Catal. **41**, 901–914 (2020).
[29]Y. Kobayashi, O. J. Hernandez, T. Sakaguchi, T. Yajima, T. Roisnel, Y. Tsujimoto, M. Morita, Y. Noda, Y. Mogami, A. Kitada, M. Ohkura, S. Hosokawa, Z. Li, K. Hayashi, Y. Kusano, J. e. Kim, N. Tsuji, A. Fujiwara, Y. Matsushita, K. Yoshimura, K. Takegoshi, M. Inoue, M. Takano, and H. Kageyama, "An oxyhydride of $BaTiO_3$ exhibiting hydride exchange and electronic conductivity," Nat. Mater. **11**, 507–511 (2012).
[30]Y. Tang, Y. Kobayashi, K. Shitara, A. Konishi, A. Kuwabara, T. Nakashima, C. Tassel, T. Yamamoto, and H. Kageyama, "On hydride diffusion in transition metal perovskite oxyhydrides investigated via deuterium exchange," Chem. Mater. **29**, 8187–8194 (2017).
[31]T. Sakaguchi, Y. Kobayashi, T. Yajima, M. Ohkura, C. Tassel, F. Takeiri, S. Mitsuoka, H. Ohkubo, T. Yamamoto, J. e. Kim, N. Tsuji, A. Fujihara, Y. Matsushita, J. Hester, M. Avdeev, K. Ohoyama, and H. Kageyama, "Oxyhydrides of (Ca, Sr, Ba)TiO_3 perovskite solid solutions," Inorg. Chem. **51**, 11371–11376 (2012).
[32]J. Kammert, J. Moon, Y. Cheng, L. Daemen, S. Irle, V. Fung, J. Liu, K. Page, X. Ma, V. Phaneuf, J. Tong, A. J. Ramirez-Cuesta, and Z. Wu, "Nature of reactive hydrogen for ammonia synthesis over a $Ru/C_{12}A_7$ electride catalyst," J. Am. Chem. Soc. **142**, 7655–7667 (2020).
[33]M. Kitano, Y. Inoue, H. Ishikawa, K. Yamagata, T. Nakao, T. Tada, S. Matsuishi, T. Yokoyama, M. Hara, and H. Hosono, "Essential role of hydride ion in ruthenium-based ammonia synthesis catalysts," Chem. Sci. **7**, 4036–4043 (2016).
[34]P.-V. Ong, L. E. Johnson, H. Hosono, and P. V. Sushko, "Structure and stability of CaH_2 surfaces: On the possibility of electron-rich surfaces in metal hydrides for catalysis," J. Mater. Chem. A **5**, 5550–5558 (2017).
[35]M. Kitano, J. Kujirai, K. Ogasawara, S. Matsuishi, T. Tada, H. Abe, Y. Niwa, and H. Hosono, "Low-temperature synthesis of perovskite oxynitride-hydrides as ammonia synthesis catalysts," J. Am. Chem. Soc. **141**, 20344–20353 (2019).
[36]Y. Kobayashi, Y. Tang, T. Kageyama, H. Yamashita, N. Masuda, S. Hosokawa, and H. Kageyama, "Titanium-based hydrides as heterogeneous catalysts for ammonia synthesis," J. Am. Chem. Soc. **139**, 18240–18246 (2017).
[37]M. Hattori, N. Okuyama, H. Kurosawa, and M. Hara, "Low-temperature ammonia synthesis on iron catalyst with an electron donor," J. Am. Chem. Soc. **145**, 7888–7897 (2023).
[38]M. Miyazaki, K. Ogasawara, T. Nakao, M. Sasase, M. Kitano, and H. Hosono, "Hexagonal $BaTiO_{(3-x)}H_x$ oxyhydride as a water-durable catalyst support for chemoselective hydrogenation," J. Am. Chem. Soc. **144**, 6453–6464 (2022).
[39]G. Kresse and J. Furthmuller, "Efficiency of ab-initio total energy calculations for metals and semiconductors using a plane-wave basis set," Comput. Mater. Sci. **6**, 15–50 (1996).
[40]G. Kresse and J. Furthmuller, "Efficient iterative schemes for *ab initio* total-energy calculations using a plane-wave basis set," Phys. Rev. B **54**, 11169–11186 (1996).
[41]J. P. Perdew, K. Burke, and M. Ernzerhof, "Generalized gradient approximation made simple," Phys. Rev. Lett. **77**, 3865–3868 (1996).
[42]S. Grimme, J. Antony, S. Ehrlich, and H. Krieg, "A consistent and accurate ab initio parametrization of density functional dispersion correction (DFT-D) for the 94 elements H-Pu," J. Chem. Phys. **132**, 154104 (2010).
[43]P. E. Blöchl, "Projector augmented-wave method," Phys. Rev. B **50**, 17953–17979 (1994).
[44]H. J. Monkhorst and J. D. Pack, "Special points for Brillouin-zone integrations," Phys. Rev. B **13**, 5188–5192 (1976).
[45]K. Momma and F. Izumi, "*VESTA* 3 for three-dimensional visualization of crystal, volumetric and morphology data," J. Appl. Crystallogr. **44**, 1272–1276 (2011).
[46]C. Ricca, I. Timrov, M. Cococcioni, N. Marzari, and U. Aschauer, "Self-consistent DFT+U study of oxygen vacancies in $SrTiO_3$," Phys. Rev. Res. **2**, 023313 (2020).
[47]Q. Wan, V. Fung, S. Lin, Z. Wu, and D.-e. Jiang, "Perovskite-supported Pt single atoms for methane activation," J. Mater. Chem. A **8**, 4362–4368 (2020).